Enhancement of Photoluminescence Quantum Yield of Silver Clusters by Heavy Atom Effect

Aoi Akiyama,[a] Sakiat Hossain,[b] Yoshiki Niihori,*[b] Kazutaka Oiwa,[a] Jayoti Roy,[c] Tokuhisa Kawawaki,[a] Thalappil Pradeep,[c] and Yuichi Negishi*[b,d]

[a] A. Akiyama, K. Oiwa, Dr. T. Kawawaki
Department of Chemistry, Graduate School of Science
Tokyo University of Science
Kagurazaka, Shinjuku-ku, Tokyo 162−8601 (Japan)

[b] Dr. S. Hossain, Dr. Y. Niihori, Prof. Y. Negishi
Research Institute for Science & Technology
Tokyo University of Science
Kagurazaka, Shinjuku-ku, Tokyo 162−8601 (Japan)
E-mail: niihori@rs.tus.ac.jp / yuichi.negishi.a8@tohoku.ac.jp

[c] Dr. J. Roy, Prof. T. Pradeep
DST Unit of Nanoscience (DST UNS) and Thematic Unit of Excellence (TUE), Department of Chemistry
Indian Institute of Technology
Madras, Chennai 600036 (India)

[d] Prof. Y. Negishi
Institute of Multidisciplinary Research for Advanced Materials
Tohoku University
Katahira, Aoba-ku, Sendai 980−8577 (Japan)
E-mail: yuichi.negishi.a8@tohoku.ac.jp

Abstract: Many ligand-protected metal clusters exhibit phosphorescence at room temperature. However, strategies for improving their phosphorescence quantum yield, a critical parameter of performance, remain poorly developed. In contrast, fluorescent dyes are commonly modified by introducing heavy atoms, such as iodine (I), to enhance intersystem crossing in the excited state, thereby harnessing the heavy atom effect to increase phosphorescence efficiency. In this study, we successfully synthesized a pair of ligand-protected silver (Ag) clusters with internal cavities encapsulating anions (X^{z-}), namely sulfide ions (S^{2-}) or iodide ions (I^{-}), which significantly differ in atomic number each other. Single-crystal X-ray diffraction and nuclear magnetic resonance spectroscopy revealed that the resulting Ag clusters were composed of $X@Ag_{54}S_{20}(thiolate)_{20}(sulfonate)_m$, where (X, m) = (S, 12) or (I, 11). X-ray photoelectron spectroscopy revealed that the Ag atoms in these compounds exhibit a mixed-valence state. Furthermore, experiments on their photoluminescence revealed that a heavy central anion induced

an internal heavy-atom effect similar to that observed in organic fluorescent dyes. As a result, the phosphorescence quantum yield became 16 times higher when S^{2-} was replaced by I^- as the central atom.

Introduction

Progress in nanotechnology is facilitated by the development of precise synthesis methods and the detailed characterization of fine and sophisticated nanomaterials. Ligand-protected metal clusters, a representative group of nanomaterials, have been the focus of numerous studies, resulting in the establishment of precise synthesis methods and the elucidation of their properties through synergistic experimental and theoretical investigations.[1] Among these, ligand-protected metal clusters composed of noble metal elements, such as gold (Au), silver (Ag), and copper (Cu), exhibit unique properties according to the number of constituent atoms and dopant elements, including photoluminescence (PL),[2] magnetic properties,[3] and catalytic activity.[4] These characteristics have attracted significant attention in both fundamental research and practical applications.[5] Recently, studies have also been conducted on clusters with complex structures arising from combinations of noble metal elements and main group elements.[6] Among these, Ag–sulfur (Ag–S) based clusters are metal clusters with cavities[7] capable of encapsulating various anions,[8] and recent efforts have focused on altering the encapsulated anionic species to modulate the physicochemical properties of these clusters.[7b, 9]

Ligand-protected metal clusters often exhibit PL.[10] Recent experimental studies have shown that phosphorescence originates in the excited triplet state.[11] Therefore, enhancing the population of the excited triplet state of metal clusters is crucial for their application as room-temperature phosphorescent materials and triplet sensitizers.[12] Generally, transition from the excited singlet state (S_n) to the excited triplet state (T_m) is spin-forbidden, resulting in a zero transition-moment. However, studies on organic fluorescent dyes have shown that introducing heavy atoms, such as iodine (I), into the fluorophore enhances spin-orbit coupling (the internal heavy-atom effect), which increases the rate constant for intersystem crossing (ISC) from S_n to T_m, thereby improving the efficiency of phosphorescence.[13] Similarly, encapsulating a heavy atom into Ag–S clusters may enhance the phosphorescence quantum yield. However, to date, there are limited reports on the internal heavy-atom effect of ligand-protected metal clusters.[14]

In this study, we successfully synthesized ligand-protected Ag–S clusters with central cavities encapsulating anions X^{z-}, where $X^{z-} = S^{2-}$ (sulfide) or I^- (iodide), which significantly differ in atomic number each other (Scheme 1). Single-crystal X-ray diffraction (SC-XRD) and proton nuclear magnetic resonance (^{1}H NMR) spectroscopy revealed that the resulting Ag clusters were composed of $X@Ag_{54}S_{20}(thiolate)_{20}(sulfonate)_m$, where (X, *m*) = (S, 12) or (I, 11) (**X@Ag54**). Furthermore, a comparison of the optical properties of the obtained pair of **X@Ag54** (X = S or I) demonstrated that an internal heavy-atom effect occurred in these Ag–S clusters, similar to that in organic fluorescent dyes. Accordingly, the phosphorescence quantum yield was 16 times higher when S^{2-} was replaced by I^- as the encapsulated atom (Scheme 1).

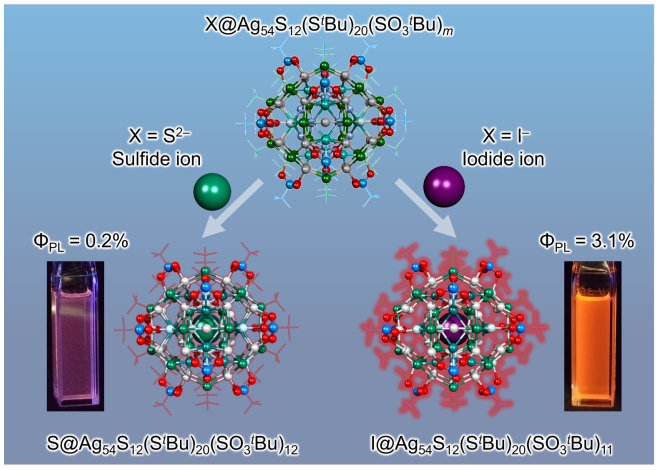

Scheme 1. Enhancement of phosphorescence quantum yield by encapsulating S^{2-} or I^{-} anions inside the central cavity of the $Ag_{54}S_{20}(S^{t}Bu)_{20}(SO_3{}^{t}Bu)_m$ framework.

Results and Discussion

Synthesis

For the synthesis of **S@Ag54**, 48.6 mg (0.22 mmol) of silver trifluoroacetate (Ag(TFA)) and 10.6 mg (0.044 mmol) of copper(II) nitrate trihydrate ($Cu(NO_3)_2{\cdot}3H_2O$) were dissolved in 4 mL of a mixture of acetone and acetonitrile (50/50 vol%). Then, 15 μL (0.13 mmol) of *tert*-butanethiol (^{t}BuSH) was added to this solution, and the resulting mixture was transferred into a glass tube (Figure S1A). A cap with a small hole (Figure S1B) was placed on the glass tube, and the tube was left undisturbed under a fluorescent lamp for light irradiation (Figure S1C). Orange crude crystals of **S@Ag54** were obtained after approximately one week (Figure S2Aa). The crude crystals were dissolved in chloroform, and hexane was slowly added to the upper layer. The solution was left to stand for one month, resulting in the formation of single crystals of **S@Ag54** (Figure S2Ba).

I@Ag54 was synthesized in the same manner as **S@Ag54**, except 20 mg (0.054 mmol) of tetrabutylammonium iodide (TBAI), as well as ^{t}BuSH, was added to the acetone/acetonitrile mixture of Ag(TFA)/$Cu(NO_3)_2$. Red-orange crude crystals of **I@Ag54** were obtained after approximately two weeks (Figure S2Ab). The crude crystals were dissolved in chloroform, and hexane was slowly added to the upper layer. The solution was left to stand for one month, resulting in the formation of single crystals of **I@Ag54** (Figure S2Bb).

Chemical composition

S@Ag54 and **I@Ag54** were crystallized in space groups of *Fm*−3 and *Pa*−3, respectively (Table S1), and their geometric structures were determined using SC-XRD (Figures 1A and 1B). According to these geometric structures, the chemical compositions of **S@Ag54** and **I@Ag54** were $X@Ag_{54}S_{20}(S^{t}Bu)_{20}(SO_3{}^{t}Bu)_m$ (X = S and I; $S^{t}Bu$ = *tert*-butanethiolate; $SO_3{}^{t}Bu$ = *tert*-butyl sulfonate) (hereafter, **X@Ag54**). Although the number of $SO_3{}^{t}Bu$ ligands in both **S@Ag54** and **I@Ag54** was determined to be 12 by SCXRD, the latter cluster exhibits relatively high thermal parameters for the

$SO_3{}^t$Bu ligands. We believe this is due to the lower occupancy of these ligands. Therefore, an attempt was made to estimate the number of $SO_3{}^t$Bu ligands in **I@Ag54** through ^{1}H NMR analysis. In the ^{1}H NMR spectra of **S@Ag54** and **I@Ag54** (Figure 2), the two peaks at 1.63 and 1.38 ppm can be attributed to the protons of S^tBu and $SO_3{}^t$Bu, respectively.[6b, 6h] The integral values of these peaks revealed that **S@Ag54** contained 12 $SO_3{}^t$Bu ligands, while **I@Ag54** contained 11 $SO_3{}^t$Bu ligands. These results indicated that the chemical compositions of **S@Ag54** and **I@Ag54** were $S@Ag_{54}S_{20}(S^tBu)_{20}(SO_3{}^tBu)_{12}$ and $I@Ag_{54}S_{20}(S^tBu)_{20}(SO_3{}^tBu)_{11}$, respectively (Figure 1).

The above chemical compositions indicate that there is a difference in the number of $SO_3{}^t$Bu ligand between **S@Ag54** and **I@Ag54**. Ligand-protected metal clusters are generally formed when the total number of valence electrons is even.[6g, 15] In this study, SC-XRD and electrospray ionization (ESI) mass spectrometry of the low mass region showed that no TFA^-, which could be a counter ion, was observed in either S@Ag54 or I@Ag54, suggesting that these clusters were neutral. In this case, because $S@Ag_{54}S_{20}(S^tBu)_{20}(SO_3{}^tBu)_{12}$ has an even number of valence electrons, **I@Ag54** with the same ligand combination ($I@Ag_{54}S_{20}(S^tBu)_{20}(SO_3{}^tBu)_{12}$) should have an odd number of valence electrons. Therefore, it can be considered that **I@Ag54** was formed with one fewer $SO_3{}^t$Bu ligand than **S@Ag54** to prevent destabilization due to the odd number of valence electrons.

To gain a deeper understanding of the chemical composition, we also acquired ESI mass spectra of the products. The ESI-mass spectra of both **S@Ag54** and **I@Ag54** contained multiple peaks attributed to ions in which AgS or ligands were adsorbed or desorbed from the clusters[16] (e.g., **I@Ag54** + 2 AgS) (Figure S3, Tables S2 and S3). These results confirmed that the estimation of the above chemical compositions is collect for both **X@Ag54**.

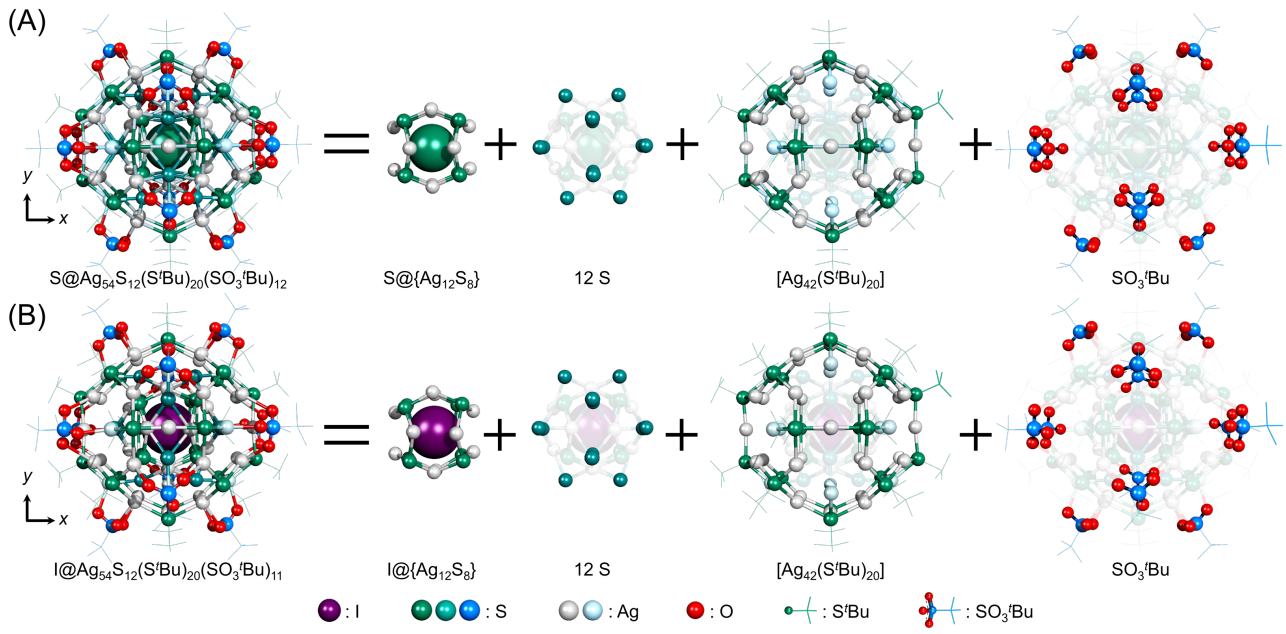

Figure 1. Geometric structures of (A) **S@Ag54** and (B) **I@Ag54**.

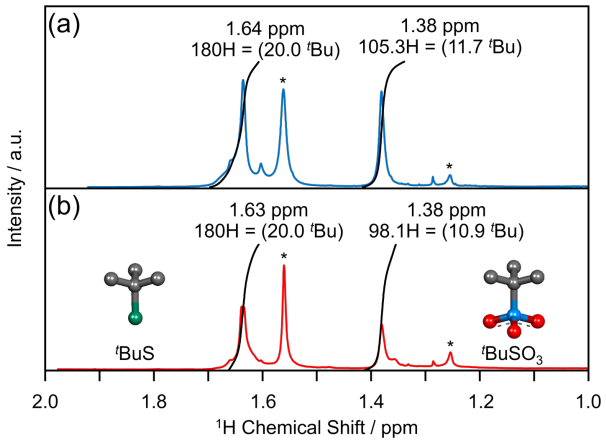

Figure 2. ^{1}H NMR spectra of (a) **S@Ag54** and (b) **I@Ag54** in $CDCl_3$. The asterisks (*) mark the peaks attributed to impurities, such as water (1.56 ppm) or alkanes/grease (1.25 ppm).

Geometric structure

The geometric structures of **X@Ag54** clusters were similar each other, with both containing an X@{$Ag_{12}S_8$} core (Figures 1A and 1B). In this core, the central anion X (S^{2-} or I^-) was surrounded by 12 Ag atoms, forming an icosahedron (point group I_h) (Figure S4), with 8 S atoms in a cubic arrangement surrounding this core. On the surface of the X@{$Ag_{12}S_8$} core, 12 S atoms formed an intermediate layer (highlighted in yellow, Figure S4A), which was connected to outer $Ag_{42}(S^tBu)_{20}$. The 12 S atoms of the intermediate layer were bonded to 12 Ag atoms of $Ag_{42}(S^tBu)_{20}$ (X@{$Ag_{12}S_8$}S_{12}[$Ag_{42}(S^tBu)_{20}$]) (highlighted in blue, Figure S4A). On the surface of X@{$Ag_{12}S_8$}S_{12}[$Ag_{42}(S^tBu)_{20}$], the S atoms of S(^{t}Bu) were arranged in a regular icosahedral structure with two coordination modes: μ_3-S(^{t}Bu) and μ_4-S(^{t}Bu) (Figure S4B and S4C). The *m* $SO_3{}^tBu$ ligands were coordinated with 12 Ag atoms of $Ag_{42}(S^tBu)_{20}$ (highlighted in blue, Figure S4A), which were bonded to the S atoms of the intermediate layer, as well as 2 Ag atoms of remaining $Ag_{30}(S^tBu)_{20}$ (highlighted in red, Figure S4A) in the coordination mode of μ_3-$O_3S(^tBu)$-κ^3O,O',O'' (Figure S4D). Owing to this structure, **X@Ag54** can be described as X@{$Ag_{12}S_8$}S_{12}[$Ag_{42}(S^tBu)_{20}(SO_3{}^tBu)_m$].

In these structures, both the X@{$Ag_{12}S_{20}$} part and surrounding $Ag_{42}(S^tBu)_{20}(SO_3{}^tBu)_m$ shell exhibit the same T_h symmetry. However, as mentioned earlier, **I@Ag54** has one fewer $SO_3{}^tBu$ ligand than **S@Ag54**. The SC-XRD results suggest that a $SO_3{}^tBu$ ligand is missing from a random site, rather than a specific site, in **I@Ag54**. Therefore, in **I@Ag54**, the 12 coordination sites are randomly occupied by 11 $SO_3{}^tBu$ ligands, leading to the formation of multiple structural isomers and accordingly, disorder in the geometric structure of **I@Ag54**.

These geometric structures of **X@Ag54** are similar to those of previously reported clusters, such as $S@Ag_{40.13}Cu_{13.87}S_{18}(S^tBu)_{20}(SO_3{}^tBu)_{12}$ and $S@Cu_{54}S_{12}O_6(S^tBu)_{20}(SO_3{}^tBu)_{12}$.[6h, 6i] In the two previously reported clusters, the $M_{42}(S^tBu)_{20}(SO_3{}^tBu)_{12}$ (M = Ag or Cu) shell, which has T_h symmetry, also covers the core. However, there are two major differences between these two previously reported clusters and **X@Ag54**: 1) in the previously reported clusters, Ag and Cu, or only Cu, are included as metals, whereas in **X@Ag54**, only Ag is present as the metal of the clusters; 2) the

previously reported clusters have two fewer chalcogenide ions (S^{2-} or O^{2-}) other than the central ion (18 chalcogenide ions) than **X@Ag54** (20 sulfide ions). As a result, the diameter of the cavity of the $M_{12}S_8$ core of **X@Ag54** (approximately 5.04 and 5.13 Å for **S@Ag54** and **I@Ag54**, respectively; Figures S4E and S5), is greater than that of the two previously reported clusters (4.94 Å and 4.88 Å).[6b-i, 17] For this reason, both S^{2-} (ionic radius = 1.84 Å) and I^- (ionic radius = 2.20 Å),[18] were stably encapsulated inside the $\{M_{12}S_8\}$ core of **X@Ag54**.

Formation mechanism

X@Ag54 contains 20 S atoms. These S atoms are considered to be produced through the reaction between Ag—S^{t}Bu and Ag^+: this reaction produces Ag_2S. [6a] In this study, although only ^{t}BuSH was added as the ligand during the synthesis, in-situ produced $SO_3{}^t$Bu was also included as a ligand in **X@Ag54**, as confirmed by SC-XRD (Figure 1), ^{1}H NMR (Figure 2), and ESI-mass spectroscopy (Figure S3), in addition to X-ray photoelectron spectroscopy (XPS) (Figures 3, S6, and S7) and Fourier-transform infrared (FT-IR) absorption spectroscopy (Figure S8), of the products. The catalytic oxidation of thiols by Cu^{2+} (Scheme S1) is responsible for the formation of these $SO_3{}^t$Bu ligands.[6h, 6i] In this reaction, Cu^{2+} coordinates with RSH, which reduces Cu (Cu^+) and generates the thiyl radical (RS·).[19] RS· reacts with oxygen molecular (O_2) and unreacted RSH in the system to produce RSO_3H (Figure S9). After coordinating with RSH, Cu^+ is oxidized to Cu^{2+} by O_2, returning to its original state. As these reactions proceed, $SO_3{}^t$Bu is formed in the reaction solvent and coordinates with the metal cluster (Scheme S1). In these reactions, the coordination and reduction of Cu^{2+} and formation of RSO_3H from RS· proceed with rate constants of approximately $10^{8–10}$ $M^{-1}s^{-1}$,[19] which is very fast. Moreover, these reactions are faster than the oxidation of Cu^+ to Cu^{2+} by O_2, which becomes the rate-limiting step. Indeed, when $Cu(NO_3)_2$ and ^{t}BuSH were mixed, the blue color of the solution immediately disappeared owing to the reduction of Cu^{2+} to colorless Cu^+, whereas this blue color took 2 days to reappear as Cu^+ reverted to Cu^{2+} (Figure S10Ba). However, when Ag^+ coexisted with Cu^{2+} and ^{t}BuSH, the recovery of Cu^{2+} from Cu^+ occurred more rapidly (Figure S10), with the disappearance of ^{t}BuSH confirmed by electron spin resonance (ESR) spectroscopy of the reaction solution. These results demonstrate that the presence of Ag^+ accelerates the rate-limiting step of RSH oxidation by Cu^{2+}, thereby accelerating the formation of RSO_3H.

Zhu et al. have reported the synthesis of $S@Ag_{40.13}Cu_{13.87}S_{18}(S^tBu)_{20}(SO_3{}^tBu)_{12}$ containing both Ag and Cu as metals under reaction conditions similar to those used in our study.[6h] However, in our study, **X@Ag54**, which contains only Ag as the metal, was synthesized (Figure 3C). In our study, unlike the research by Zhu et al., we did not add the reducing reagents, such as borane amine complexes,[6h] into the reaction solvent. Moreover, compared to their study, we significantly reduced the amount of Cu^{2+} catalyst relative to Ag^+ (1.260 vs 0.198 atom %). These factors likely contributed to the successful synthesis of **X@Ag54** with only Ag as the metal, which enabled the encapsulation of I^-.

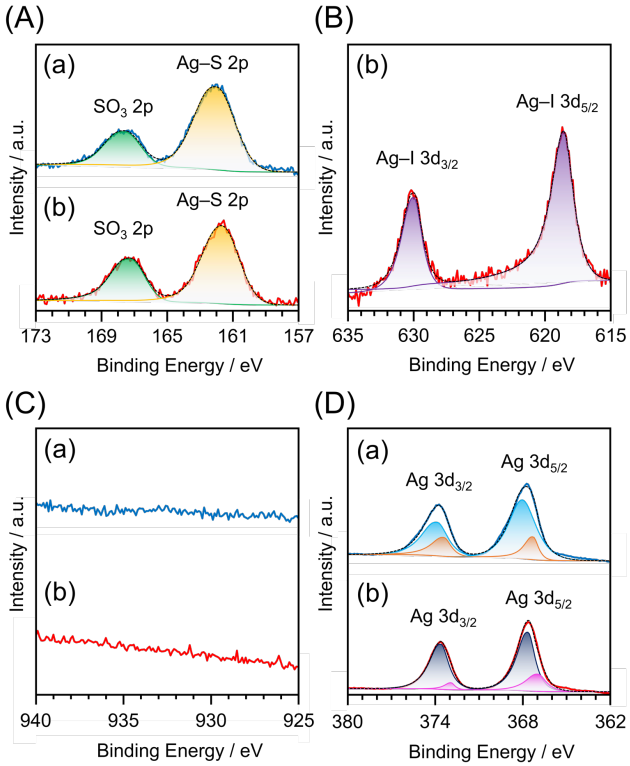

Figure 3. X-ray photoelectron spectra of (A) S 2p, (B) I 3d, (C) Cu 2p, (D) and Ag 3d for (a) **S@Ag54** and (b) **I@Ag54**. Different colors of fitting curves in spectra correspond to different oxidation states. In (A), the peaks on the low binding energy side (yellow) are attributed to sulfide S^{2-} or thiolate $^{t}BuS^{-}$, and the peaks on the high binding energy side (green) are attributed to S derived from sulfonate $^{t}BuSO_3^{-}$. Spectrum (B) indicates that the charge state of I is similar to that of I^{-}. Spectrum (C) indicates that **X@Ag54** does not include Cu. In (D), the peaks around 368 eV and 374 eV are attributed to Ag $3d_{5/2}$ and Ag $3d_{3/2}$, respectively. These spectra indicated that the oxidation state of Ag in **X@Ag54** was similar to that of Ag_2S and AgO.

Oxidation state of Ag

The core of **X@Ag54** consisted of only Ag and S and formed a central cavity, as observed in previously reported $[S@Ag_{50}S_{12}(S^{t}Bu)_{20}](TFA)_4$.[6c] In the previously reported cluster, all the Ag atoms are in the +1 oxidation state, giving rise to a single sharp peak in both the Ag $3d_{3/2}$ and $3d_{5/2}$ regions of its XPS spectrum. In contrast, broad peaks were observed in the Ag $3d_{5/2}$ and $3d_{3/2}$ regions of the XPS spectra of **X@Ag54** (Figure 3D). These peaks were fitted with two functions, and the position of the peak on the high-energy side was close to the position of the peak corresponding to Ag_2S or AgO (Figures 3D and S6, Table S4).[20] These observations indicates that Ag in **X@Ag54** is in a mixed-valence state, rather than the single-valence state of Ag in $[S@Ag_{50}S_{12}(S^{t}Bu)_{20}](TFA)_4$.[6c] In fact, there have been several reports on Ag existing in mixed-valence states.[20-21] For example, bulk silver monoxide (AgO), which can be described as $Ag_2O{\cdot}Ag_2O_3$, contains Ag in a mixed-valence state of Ag^{I} and Ag^{III}.[21c, 22] Furthermore, Cu atoms in Cu–chalcogen clusters with geometric structures similar to those of **X@Ag54**, such as $[S@Cu_{54}S_{12}O_6(S^{t}Bu)_{20}(SO_3{}^{t}Bu)_{12}]$ and

$[Cu_{50}S_{12}(S^tBu)_{20}(TFA)_{12}]$, also exist in a mixed-valence state of Cu^I and Cu^{II}.[6b, 6i, 23] Unlike $[S@Ag_{50}S_{12}(S^tBu)_{20}](TFA)_4$, **X@Ag54** contained two types of ligands (S^tBu and $SO_3{}^tBu$), and this can be considered to cause the mixed-valence state of Ag.

Stability

To apply the clusters as materials, information on their stability is crucial. Therefore, the stability of **X@Ag54** against the following three factors was investigated: 1) degradation in solution, 2) heat-induced dissociation, and 3) collision-induced dissociation (CID).

Stability against degradation in solution was evaluated by heating **X@Ag54** in toluene and tracking changes in its ultraviolet–visible (UV–vis) absorption spectrum. The results showed that 1) the stabilities of both clusters are similar, and 2) the absorption spectra of both samples in toluene can remain unchanged over 20 h of heating at 60 °C (Figures 4Aa, 4Ab, and S11). The half-life of both clusters under these degradation conditions was estimated to be approximately 200 h (Table S5).

Stability against heat-induced dissociation was evaluated using thermogravimetric analysis (TGA). Both clusters underwent three stages of weight loss (Figures 4Ba, 4Bb, and S12). According to the weight of the ligands and their functional groups, the weight loss at approximately 100 °C is attributed to the removal of $SO_3{}^tBu$ ligands (theoretical loss = 20% for **S@Ag54** and 16% for **I@Ag54**), while the weight loss at approximately 120 °C is attributed to the removal of ^tBu groups from S^tBu ligands (theoretical loss = 11% for both **S@Ag54** and **I@Ag54**). The final weight loss at approximately 180 °C is interpreted as the removal of sulfur (theoretical loss = 6.5% for both **S@Ag54** and **I@Ag54**). The slow weight loss at subsequent temperatures can be attributed to the desorption of sulfur or X from the remaining $X@Ag_{54}S_{20}$. The dissociation energies of Ag—$SO_3{}^tBu$ and AgS—^tBu, calculated using density functional theory (DFT), were 54.2 and 57.4 kcal/mol, respectively (Table S6). This should be the reason why thermal dissociation occurred in the order. The initial loss of $SO_3{}^tBu$ occurred at 133 °C for **S@Ag54** and at 135 °C for **I@Ag54**. The subsequent weight loss also occurred at similar temperatures. These results indicates that the stability of both clusters against thermal dissociation is similar each other.

Stability against CID was investigated in a vacuum.[24] Specifically, **X@Ag54** was introduced into an ESI-mass spectrometer, where it collided with argon (Ar) to undergo CID. The stability of each cluster was examined by evaluating the chemical composition and ion intensity of the generated fragment ions. Mass spectra were obtained following the collision of [**S@Ag54** + $SO_3{}^tBu]^{2+}$ and [**I@Ag54** + $SO_3{}^tBu$ + 2AgS]$^{2+}$ with Ar at different collision energies (Figure 5A and 5B, Table S9). The parent ions of **X@Ag54** dissociated as the collision energy increased. The main dissociation patterns corresponded to the radical cleavage of Ag—O_3S^tBu and S—^tBu (Figure 5C). These dissociation patterns closely resembled those observed in the TGA curves. Furthermore, these dissociation reactions of both clusters occurred at similar collision energies (Figures S13 and S14, Tables S7 and S8), indicating that the stability of both clusters against CID was also similar each other.

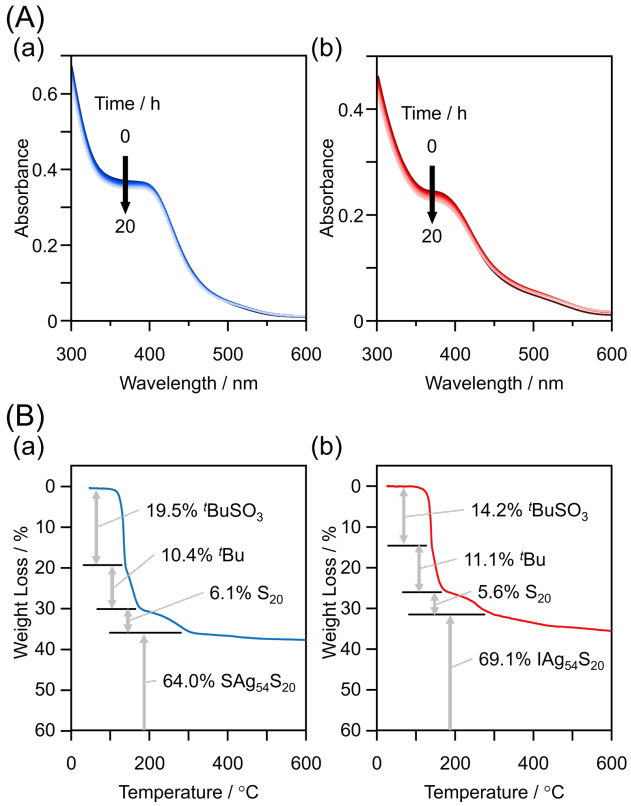

Figure 4. Stability of **X@Ag54**. (A) Time evolution of the absorption spectrum of toluene solutions of (a) **S@Ag54** and (b) **I@Ag54** at 60 °C. (B) TGA curves of (a) **S@Ag54** and (b) **I@Ag54**.

In these experiments, detachment of surface ligands was the first step of degradation. It can be considered that since the difference in the kinds of the central anions (X) do not significantly affect the binding energy between surface Ag and the ligands, the two **X@Ag54** clusters showed similar stability against the three factors tested in the above experiments.

Photoluminescence

Figure 6A shows the PL spectra of **X@Ag54** in toluene under an Ar atmosphere. To obtain strong PL, the excitation wavelength was set to 405 nm. Both cluster solutions exhibited a broad PL peak at approximately 610 nm (Figure S15). Recent studies have shown that the PL of metal clusters consisting of a large number of metal atoms entails photoexcitation to generate a dark excited singlet state, which subsequently undergoes intersystem crossing (ISC) to a bright excited triplet state, resulting in phosphorescence.[11, 12c 25] Because **X@Ag54** also comprised a large number of metal atoms, the observed emission of **X@Ag54** is likely phosphorescence. In fact, the estimated radiative lifetime of **X@Ag54** was on the order of tens to hundreds of microseconds (Table 1), which is significantly longer than that of fluorescent materials (≤ 1 μs).[26]

The photoluminescence quantum yield (Φ_{PL}) of **X@Ag54** was evaluated using a relative method,[27] revealing that the Φ_{PL} of **I@Ag54** was approximately 16 times greater than that of

S@Ag54 (Table 1). Because there was no significant difference in the symmetry of the geometries of the two **X@Ag54** clusters, the difference in Φ_{PL} did not arise from symmetry breaking.[28]

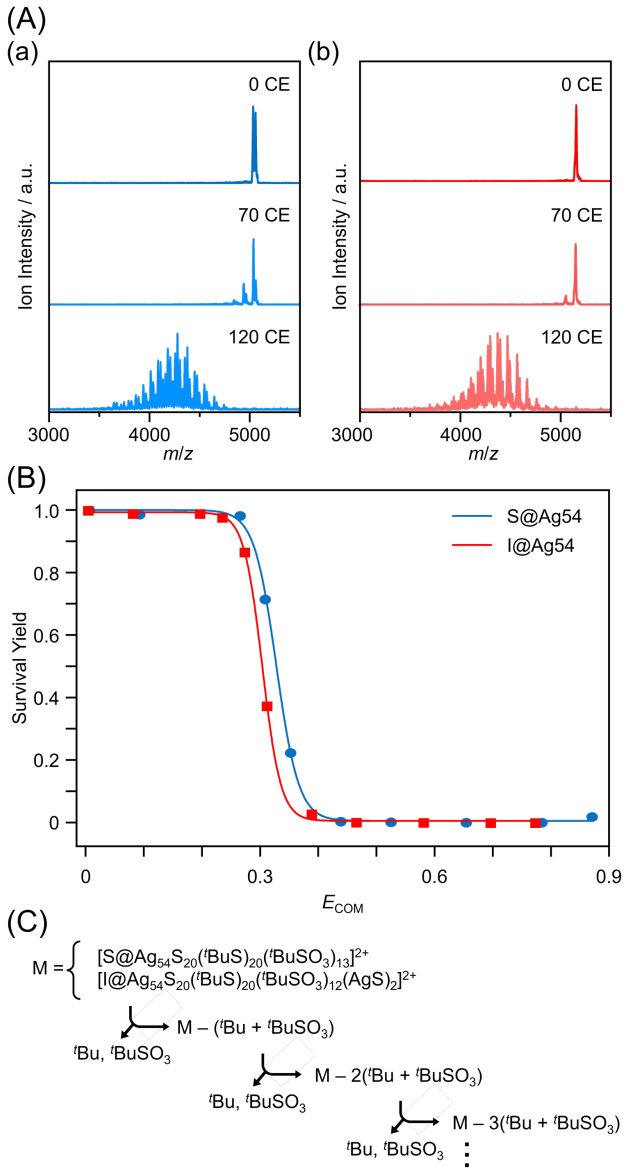

Figure 5. (A) CID-mass spectra of (a) **S@Ag54** and (b) **I@Ag54** as a function of collision energy. CE indicates the collision energy. (B) Survival yield obtained from CID profiles of **X@Ag54** (Figure 5A). Details for calculating the survival yield are provided in the Supporting Information (Section S1.8). (C) CID process of **X@Ag54**.

Table 1. Photoluminescence properties of **X@Ag54**.

Sample	Φ_{PL}	τ_{PL} (ns)	k_r (s^{-1})	k_{nr} (s^{-1})	τ_r (μs)
S@Ag54	2.0×10^{-3}	106.2	1.9×10^{3}	9.4×10^{6}	530
I@Ag54	3.1×10^{-2}	652.9	4.8×10^{4}	1.5×10^{6}	21

Φ_{PL}, PL quantum yield; τ_{PL}, averaged PL lifetime, k_r, radiative rate constant; k_{nr}, nonradiative rate constant; τ_r, radiative lifetime (reciprocal of k_r).

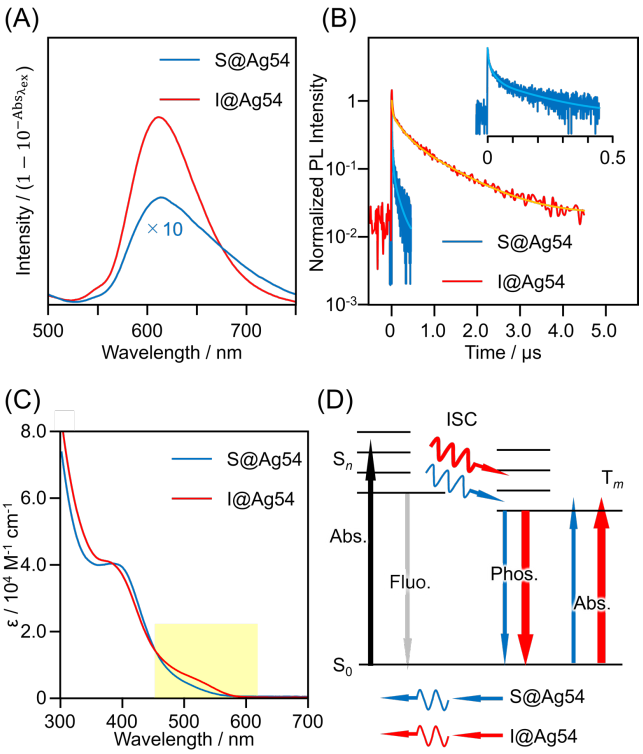

Figure 6. (A) PL spectra of deuterated toluene solutions of **X@Ag54**. Excitation wavelength was fixed at 405 nm. Vertical axis is the PL intensity divided by the transmittance of the sample at the excitation light wavelength. (B) PL decay curves of deuterated toluene solutions of **X@Ag54**. Excitation wavelength of pulse laser was fixed at 405 nm. (C) UV–vis absorption spectra of toluene solutions of **S@Ag54** and **I@Ag54**. ε represents molar absorption coefficient. The yellow part highlights the absorption assignable to S–T transition. (D) Predicted scheme of the relaxation and absorption for **X@Ag54**.

However, 1) the two **X@Ag54** clusters differs in the type of anion present in their internal cavities, and 2) Φ_{PL} increases with increasing atomic number of encapsulated anion. Introducing heavy halogens (heavy atoms) into aromatic dyes, such as acene-based compounds, enhances ISC from the excited singlet to the excited triplet state owing to the heavy atom effect, which increases the radiative rate constant (k_r) and, consequently, Φ_{PL}.[29] In the present system, a similar effect likely occurred for **I@Ag54** to exhibit photoluminescence with high Φ_{PL}.

To confirm the presence of an internal heavy-atom effect, the PL decay curves of **X@Ag54** in deuterated toluene were evaluated using the time-correlated single-photon counting method (Figure 6B). The obtained decay curves were fitted with multiple exponential decays to determine the average photoluminescence lifetimes (τ_{PL}) of **S@Ag54** and **I@Ag54**, which were 106.2 and 652.9 ns, respectively (Tables 1 and S10). From this fitting, the radiative rate constants (k_r) of **I@Ag54** and

S@Ag54 were estimated to be 1.9×10^3 and 4.8×10^4 s^{-1}, respectively (Table 1). Therefore, when X changed from S^{2-} to I^-, k_r increased by approximately 25 times. This trend is similar to the enhancement of phosphorescent parameters through the heavy atom effect in conventional fluorescent dyes. Therefore, it can be interpreted that replacing S^{2-} with heavier I^- as X in **X@Ag54** accelerated ISC via the heavy atom effect,[30] which increases the population of the bright triplet state and k_r, thereby improving the Φ_{PL} of **X@Ag54**.

The non-radiative rate constant (k_{nr}) of **I@Ag54** was approximately 1/6 of that of **S@Ag54** (Table 1). Because I^- has a larger ionic radius than S^{2-}, it fills a greater volume of the cavity than S^{2-}, and thus **I@Ag54** seems to have a more rigid framework than **S@Ag54**. In addition, the bond enthalpies of Ag—I and Ag—S bonds are 234 and 217 kJ mol^{-1}, respectively, indicating that the Ag—I bond has a slightly higher bond energy than the Ag—S bond.[31] These factors seems to accelerate the vibrational relaxation of **I@Ag54** compared with that of **S@Ag54**, thereby reducing the non-radiative rate constant of **I@Ag54** to approximately 1/6 of that of **S@Ag54**.

Optical absorption

Finally, we discuss about the optical absorption of **S@Ag54** and **I@Ag54** (Figure 6C). Both spectra exhibited shoulder-like absorptions around 400 and 550 nm, and their overall optical absorption spectra were quite similar each other. However, upon closer inspection, the spectrum of **I@Ag54** contained a more distinct shoulder-like peak at approximately 500 nm compared with the spectrum of **S@Ag54**. The heavy atom effect increases the oscillator strength of the spin-forbidden transition from the ground state to the triplet excited state ($S_0\rightarrow T_1$), leading to the S−T absorption peak in the absorption spectrum.[32] In fact, in the optical absorption spectrum of some ligand-protected metal clusters, absorption peak attributable to S−T transition appears with a relatively high oscillator strength at a slightly longer wavelength than the peak attributed to $S_0\rightarrow S_n$ transition.[11] Therefore, we predict that the shoulder peak at approximately 500 nm in the optical absorption spectrum of **X@Ag54** is derived from S−T absorption, which is promoted by the heavy atom effect (Figure 6D). The assignment of these optical absorption peaks is expected to be clarified through DFT calculations[33] in future studies.

Conclusion

In this study, we successfully synthesized a pair of **X@Ag54** clusters (X = S or I) protected by two types of ligands, thiolate and sulfonate, by adding Ag^+ and a catalytic amount of Cu^{2+} to the reaction system. No significant difference was observed between the two **X@Ag54** clusters (X = S or I) in terms of geometric structure and stability against degradation. However, notable differences were observed in their PL and optical absorption. We concluded that the differences in their optical properties are derived from the heavy atom effect. This effect enhances the oscillator strength of transitions from the spin-forbidden excited singlet state to the triplet excited state, as well as transitions from the ground singlet state to the triplet excited state. This study clearly demonstrated that incorporating heavy atoms into Ag–S clusters significantly enhances their phosphorescence

quantum yield, similar to organic fluorescent dyes. These findings are expected to provide clear design guidelines for developing metal clusters as room-temperature phosphorescent materials and triplet sensitizers.

Acknowledgements

We thank Dr. Tatsuo Nakagawa and Toshiaki Suzuki (UNISOKU Co., Ltd.) for measurements of PL decay curves. We also thank Dr. Sourav Biswas for valuable comments on the valence electron model of **X@Ag54**. The computation was performed using Research Center for Computational Science, Okazaki, Japan (Project: 24-IMS-C282). This research was financially supported by the Japan Society for the Promotion of Science (JSPS) KAKENHI (grant nos. 22K04858, 22K19012, 23KK0098, and 23H00289), Yazaki Memorial Foundation for Science and Technology, and The Sumitomo Foundation.

Keywords: Precise synthesis • Ligand-protected clusters • Anion templating • Heavy atom effect • Phosphorescence

References

[1] a) M. Sera, S. Hossain, S. Yoshikawa, K. Takemae, A. Ikeda, T. Tanaka, T. Kosaka, Y. Niihori, T. Kawawaki, Y. Negishi, *J. Am. Chem. Soc.* **2024**, *146*, 29684-29693; b) T. Kawawaki, Y. Mitomi, N. Nishi, R. Kurosaki, K. Oiwa, T. Tanaka, H. Hirase, S. Miyajima, Y. Niihori, D. J. Osborn, T. Koitaya, G. F. Metha, T. Yokoyama, K. Iida, Y. Negishi, *Nanoscale* **2023**, *15*, 7272-7279; c) H. Qian, M. Zhu, Z. Wu, R. Jin, *Acc. Chem. Res.* **2012**, *45*, 1470-1479; d) Y. Negishi, H. Horihata, A. Ebina, S. Miyajima, M. Nakamoto, A. Ikeda, T. Kawawaki, S. Hossain, *Chem. Sci.* **2022**, *13*, 5546-5556.

[2] a) Y. Zhong, J. Zhang, T. Li, W. Xu, Q. Yao, M. Lu, X. Bai, Z. Wu, J. Xie, Y. Zhang, *Nat. Commun.* **2023**, *14*, 658; b) S. Takano, H. Hirai, T. Nakashima, T. Iwasa, T. Taketsugu, T. Tsukuda, *J. Am. Chem. Soc.* **2021**, *143*, 10560-10564; c) W. Ishii, Y. Okayasu, Y. Kobayashi, R. Tanaka, S. Katao, Y. Nishikawa, T. Kawai, T. Nakashima, *J. Am. Chem. Soc.* **2023**, *145*, 11236-11244; d) D. A. Buschmann, H. Hirai, T. Tsukuda, *Inorg. Chem. Front.* **2024**, *11*, 6694-6710; e) H. Liu, G. Hong, Z. Luo, J. Chen, J. Chang, M. Gong, H. He, J. Yang, X. Yuan, L. Li, X. Mu, J. Wang, W. Mi, J. Luo, J. Xie, X.-D. Zhang, *Adv. Mater.* **2019**, *31*, 1901015.

[3] a) M. Agrachev, S. Antonello, T. Dainese, J. A. Gascón, F. Pan, K. Rissanen, M. Ruzzi, A. Venzo, A. Zoleo, F. Maran, *Chem. Sci.* **2016**, *7*, 6910-6918; b) M. Zhu, C. M. Aikens, M. P. Hendrich, R. Gupta, H. Qian, G. C. Schatz, R. Jin, *J. Am. Chem. Soc.* **2009**, *131*, 2490-2492.

[4] a) E. L. Albright, T. I. Levchenko, V. K. Kulkarni, A. I. Sullivan, J. F. DeJesus, S. Malola, S. Takano, M. Nambo, K. Stamplecoskie, H. Häkkinen, T. Tsukuda, C. M. Crudden, *J. Am. Chem. Soc.* **2024**, *146*, 5759-5780; b) M. Brust, M. Walker, D. Bethell, D. J. Schiffrin, R. Whyman, *J. Chem. Soc., Chem. Commun.* **1994**, 801-802; c) K. Sakamoto, S. Masuda, S. Takano, T. Tsukuda, *ACS Catal.* **2023**, *13*, 3263-3271; d) A. V. Artem'ev, C. W. Liu, *Chem. Commun.* **2023**, *59*, 7182-7195.

[5] a) S. Li, D. Alfonso, A. V. Nagarajan, S. D. House, J. C. Yang, D. R. Kauffman, G. Mpourmpakis, R. Jin, *ACS Catal.* **2020**, *10*, 12011-12016; b) P. D. Jadzinsky, G. Calero, C. J. Ackerson, D. A. Bushnell, R. D. Kornberg, *Science* **2007**, *318*, 430-433; c) S. Knoppe, T. Bürgi, *Acc. Chem. Res.* **2014**, *47*, 1318-1326; d) Y. Negishi, K. Nobusada, T. Tsukuda, *J. Am. Chem. Soc.* **2005**, *127*, 5261-5270; e) S.-F. Yuan, C.-Q. Xu, W.-D. Liu, J.-X. Zhang, J. Li, Q.-M. Wang, *J. Am. Chem. Soc.* **2021**, *143*, 12261-12267.

[6] a) Z.-A. Nan, Y. Xiao, X.-Y. Liu, T. Wang, X.-L. Cheng, Y. Yang, Z. Lei, Q.-M. Wang, *Chem. Commun.* **2019**, *55*, 6771-6774; b) C. Xu, Y. Jin, H. Fang, H. Zheng, J. C. Carozza, Y. Pan, P.-J. Wei, Z. Zhang, Z. Wei, Z. Zhou, H. Han, *J. Am. Chem. Soc.* **2023**, *145*, 25673-25685; c) S. Biswas, A. K. Das, A. C. Reber, S. Biswas, S. Bhandary, V. B. Kamble, S. N. Khanna, S. Mandal, *Nano Lett.* **2022**, *22*, 3721-3727; d) Z.-A. Nan, Y. Wang, Z.-X. Chen, S.-F. Yuan, Z.-Q. Tian, Q.-M. Wang, *Commun. Chem.* **2018**, *1*, 99; e) D. Sun, H. Wang, H.-F. Lu, S.-Y. Feng, Z.-W. Zhang, G.-X. Sun, D.-F. Sun, *Dalton Trans.* **2013**, *42*, 6281-6284; f) S. Jin, S. Wang, Y. Song, M. Zhou, J. Zhong, J. Zhang, A. Xia, Y. Pei, M. Chen, P. Li, M. Zhu, *J. Am. Chem. Soc.* **2014**, *136*, 15559-15565; g) G. Li, Z. Lei, Q.-M. Wang, *J. Am. Chem. Soc.* **2010**, *132*, 17678-17679; h) S. Yang, J. Chai, H. Chong, Y. Song, H. Yu, M. Zhu, *Chem. Commun.* **2018**, *54*, 4314-4316; i) L.-J. Liu, J.-W. Zhang, M. Asad, Z.-Y. Wang, S.-Q. Zang, T. C. W. Mak, *Chem. Commun.* **2021**, *57*, 5586-5589; j) F. Ma, K. A. Abboud, C. Zeng, *Nat. Synth.* **2023**, *2*, 949-959.

[7] a) J.-W. Liu, L. Feng, H.-F. Su, Z. Wang, Q.-Q. Zhao, X.-P. Wang, C.-H. Tung, D. Sun, L.-S. Zheng, *J. Am. Chem. Soc.* **2018**, *140*, 1600-1603; b) L.-P. Cheng, Z. Wang, Q.-Y. Wu, H.-F. Su, T. Peng, G.-G. Luo, Y.-A. Li, D. Sun, L.-S. Zheng, *Chem. Commun.* **2018**, *54*, 2361-2364.

[8] a) Z. Wang, H.-F. Su, X.-P. Wang, Q.-Q. Zhao, C.-H. Tung, D. Sun, L.-S. Zheng, *Chem. - Eur. J.* **2018**, *24*, 1640-1650; b) C. W. Liu, H.-W. Chang, P.-K. Liao, C.-S. Fang, J.-Y. Saillard, S. Kahlal, *J. Cluster Sci.* **2011**, *22*, 381-396; c) Y. Horita, M. Ishimi, Y. Negishi, *Sci. Technol. Adv. Mater.* **2023**, *24*, 2203832.

[9] a) J.-H. Liao, C. Latouche, B. Li, S. Kahlal, J.-Y. Saillard, C. W. Liu, *Inorg. Chem.* **2014**, *53*, 2260-2267; b) Y. Horita, S. Hossain, M. Ishimi, P. Zhao, M. Sera, T. Kawawaki, S. Takano, Y. Niihori, T. Nakamura, T. Tsukuda, M. Ehara, Y. Negishi, *J. Am. Chem. Soc.* **2023**, *145*, 23533-23540.

[10] a) H. Hirai, S. Takano, T. Nakashima, T. Iwasa, T. Taketsugu, T. Tsukuda, *Angew. Chem., Int. Ed.* **2022**, *61*, e202207290; b) X. Kang, M. Zhou, S. Wang, S. Jin, G. Sun, M. Zhu, R. Jin, *Chem. Sci.* **2017**, *8*, 2581-2587; c) J.-S. Yang, Z. Han, X.-Y. Dong, P. Luo, H.-L. Mo, S.-Q. Zang, *Angew. Chem., Int. Ed.* **2020**, *59*, 11898-11902; d) M. Hesari, Z. Ding, *J. Am. Chem. Soc.* **2021**, *143*, 19474-19485.

[11] M. Mitsui, Y. Wada, R. Kishii, D. Arima, Y. Niihori, *Nanoscale* **2022**, *14*, 7974-7979.

[12] a) W.-M. He, Z. Zhou, Z. Han, S. Li, Z. Zhou, L.-F. Ma, S.-Q. Zang, *Angew. Chem., Int. Ed.* **2021**, *60*, 8505-8509; b) Y. Niihori, T. Kosaka, Y. Negishi, *Mater. Horiz.* **2024**, *11*, 2304-2322; c) D. Arima, M. Mitsui, *J. Am. Chem. Soc.* **2023**, *145*, 6994-7004; d) W.-D. Si, C. Zhang, M. Zhou, W.-D. Tian, Z. Wang, Q. Hu, K.-P. Song, L. Feng, X.-Q. Huang, Z.-Y. Gao, C.-H. Tung, D. Sun, *Sci. Adv.* **2023**, *9*, eadg3587.

[13] a) A. Rodriguez-Serrano, V. Rai-Constapel, M. C. Daza, M. Doerr, C. M. Marian, *Phys. Chem. Chem. Phys.* **2015**, *17*, 11350-11358; b) Y. He, J. Wang, Q. Li, S. Qu, C. Zhou, C. Yin, H. Ma, H. Shi, Z. Meng, Z. An, *Adv. Opt. Mater.* **2023**, *11*, 2201641.

[14] H. Hirai, S. Takano, S. Masuda, T. Tsukuda, *ChemElectroChem* **2024**, *11*, e202300669.

[15] M. Walter, J. Akola, O. Lopez-Acevedo, P. D. Jadzinsky, G. Calero, C. J. Ackerson, R. L. Whetten, H. Grönbeck, H. Häkkinen, *Proc. Natl. Acad. Sci. U. S. A.* **2008**, *105*, 9157-9162.

[16] a) R. K. Gupta, L. Li, Z. Wang, B.-L. Han, L. Feng, Z.-Y. Gao, C.-H. Tung, D. Sun, *Chem. Sci.* **2023**, *14*, 1138-1144; b) C. Zhu, J. Xin, J. Li, H. Li, X. Kang, Y. Pei, M. Zhu, *Angew. Chem., Int. Ed.* **2022**, *61*, e202205947.

[17] X. Sun, B. Yan, X. Gong, Q. Xu, Q. Guo, H. Shen, *Chem. - Eur. J.* **2024**, *30*, e202400527.

[18] R. D. Shannon, *Acta Crystallogr., Sect. A* **1976**, *A32*, 751-767.

[19] a) R. C. Smith, V. D. Reed, W. E. Hill, *Phosphorus, Sulfur Silicon Relat. Elem.* **1994**, *90*, 147-154; b) G. Saez, P. J. Thornalley, H. A. O. Hill, R. Hems, J. V. Bannister, *Biochim. Biophys. Acta, Gen. Subj.* **1982**, *719*, 24-31.

[20] a) K. Yonesato, S. Yamazoe, D. Yokogawa, K. Yamaguchi, K. Suzuki, *Angew. Chem., Int. Ed.* **2021**, *60*, 16994-16998; b) N. Haraguchi, T. Okunaga, Y. Shimoyama, N. Ogiwara, S. Kikkawa, S. Yamazoe, M. Inada, T. Tachikawa, S. Uchida, *Eur. J. Inorg. Chem.* **2021**, *2021*, 1531-1535; c) H.-H. Wang, J. Wei, F. Bigdeli, F. Rouhani, H.-F. Su, L.-X. Wang, S. Kahlal, J.-F. Halet, J.-Y. Saillard, A. Morsali, K.-G. Liu, *Nanoscale* **2023**, *15*, 8245-8254.

[21] a) E. Nag, S. Battuluri, K. Chandra Mondal, S. Roy, *Chem. - Eur. J.* **2022**, *28*, e202202324; b) Y. Jin, C. Zhang, X.-Y. Dong, S.-Q. Zang, T. C. W. Mak, *Chem. Soc. Rev.* **2021**, *50*, 2297-2319; c) X.-Y. Wang, W. Meng, H.-P. Xie, D.-N. Song, M.-H. Du, J.-X. Chen, P. Braunstein, J.-P. Lang, *Inorg. Chem.* **2024**, *63*, 13014-13021.

[22] a) D. Tudela, *J. Chem. Educ.* **2008**, *85*, 863; b) N. N. Greenwood, A. Earnshaw, *Chemistry of the Elements*, 2nd ed., Butterworth-Heinemann, Oxford, **1997**, pp. 1173-1200; c) J. P. Allen, D. O. Scanlon, G. W. Watson, *Phys. Rev. B* **2010**, *81*, 161103.

[23] D.-N. Yu, Z.-X. Yao, F. Bigdeli, X.-M. Gao, X. Cheng, J.-Z. Li, J.-W. Zhang, W. Wang, Z.-J. Guan, Y. Bu, K.-G. Liu, A. Morsali, *Inorg. Chem.* **2023**, *62*, 401-407.

[24] a) J. Roy, P. Chakraborty, G. Paramasivam, G. Natarajan, T. Pradeep, *Phys. Chem. Chem. Phys.* **2022**, *24*, 2332-2343; b) Y. Fujiwara, S. Ito, K. Koyasu, T. Tsukuda, *J. Phys. Chem. A* **2024**, *128*, 3119-3125; c) S. Ito, K. Koyasu, S. Takano, T. Tsukuda, *J. Phys. Chem. C* **2020**, *124*, 19119-19125; d) R. Tomihara, K. Hirata, H. Yamamoto, S. Takano, K. Koyasu, T. Tsukuda, *ACS Omega* **2018**, *3*, 6237-6242.

[25] a) Y. Niihori, Y. Wada, M. Mitsui, *Angew. Chem., Int. Ed.* **2021**, *60*, 2822-2827; b) M. Mitsui, D. Arima, Y. Kobayashi, E. Lee, Y. Niihori, *Adv. Opt. Mater.* **2022**, *10*, 2200864; c) M. Mitsui, D. Arima, A. Uchida, K. Yoshida, Y. Arai, K. Kawasaki, Y. Niihori, *J. Phys. Chem. Lett.* **2022**, *13*, 9272-9278; d) K. Yoshida, D. Arima, M. Mitsui, *J. Phys. Chem. Lett.* **2023**, *14*, 10967-10973; e) M. Mitsui, A. Uchida, *Nanoscale* **2024**, *16*, 3053-3060; f) M. Mitsui, Y. Miyoshi, D. Arima, *Nanoscale* **2024**, *16*, 14757-14765.

[26] N. J. Turro, V. Ramamurthy, J. C. Scaiano, *Principles of Molecular Photochemistry: An Introduction*, University Science Books, California, **2009**, p. 218.

[27] V. Bernard, M. Berberan-Santos, *Molecular fluorescence: principles and applications,* 2nd ed., Wiley-VCH, Singapore, **2013**, p. 44.

[28] E. Khatun, A. Ghosh, P. Chakraborty, P. Singh, M. Bodiuzzaman, P. Ganesan, G. Nataranjan, J. Ghosh, S. K. Pal, T. Pradeep, *Nanoscale* **2018**, *10*, 20033-20042.

[29] a) V. Bernard, M. Berberan-Santos, *Molecular fluorescence: principles and applications*, 2nd ed., Wiley-VCH, Singapore, **2012**, pp. 77-78; b) V. R. N. J. Turro, J. C. Scaiano, *Modern Molecular Photochemistry of Organic Molecules*, Wiley-VCH, Singapore, **2011**, p. 312.

[30] a) N. N. Greenwood, A. Earnshaw, *Chemistry of the Elements*, 2nd ed., Butterworth-Heinemann, Oxford, **1997**, pp. 645-746; b) W. C. Martin, *J. Res. Natl. Bur. Stand., Sect. A* **1971**, *75A*, 109-111.

[31] Y.-R. Luo, *Comprehensive Handbook of Chemical Bond Energies*, 1st ed., CRC Press, Boca Raton, **2007**, p. 60.

[32] M. Nakajima, S. Nagasawa, K. Matsumoto, T. Kuribara, A. Muranaka, M. Uchiyama, T. Nemoto, *Angew. Chem., Int. Ed.* **2020**, *59*, 6847-6852.

[33] a) B. D. Peter, W. Pei, G. N. Andrew, S. Zhou, Z. Luo, *Nanoscale* **2024**, *16*, 8090-8095; b) K. Maghrebi, I. Chantrenne, S. Messaoudi, T. Frauenheim, A. Fihey, C. R. Lien-Medrano, *J. Phys. Chem. C* **2023**, *127*, 19675-19686; c) K. Li, P. Wang, Y. Pei, *J. Phys. Chem. Lett.* **2024**, *15*, 9216-9225; d) E. L. Albright, S. Malola, S. I. Jacob, H. Yi, S. Takano, K. Mimura, T. Tsukuda, H. Häkkinen, M. Nambo, C. M. Crudden, *Chem. Mater.* **2024**, *36*, 1279-1289; e) S. Havenridge, C. M. Aikens, *J. Phys. Chem. A* **2023**, *127*, 9932-9943; f) T. Okada, T. Kawawaki, K. Takemae, S. Tomihari, T. Kosaka, Y. Niihori, Y. Negishi, *J. Phys. Chem. Lett.* **2024**, *15*, 1539-1545.

Entry for the Table of Contents

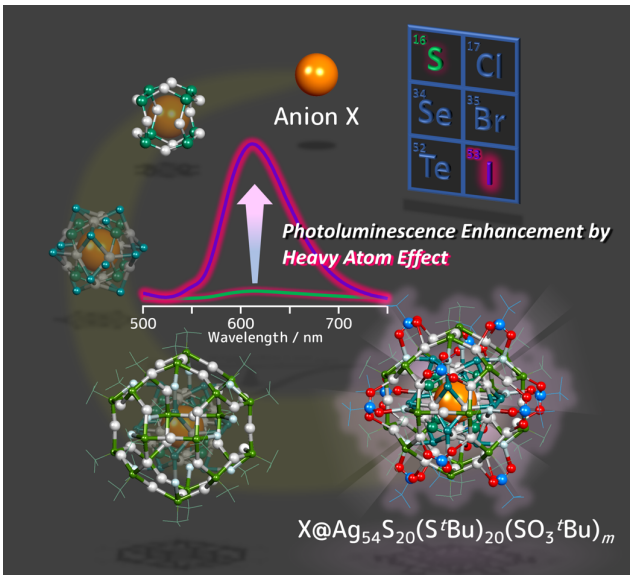

Novel Ag54 clusters, composed of silver and sulfur and protected by thiolate and sulfonate, has a large internal cavity that can encapsulate sulfide and iodide ions. The encapsulation of iodide ions into Ag54 enhances the spin-orbit interaction and improves phosphorescence properties.